Rapid Folding of DNA into Nanoscale Shapes at Constant Temperature

Jean-Philippe J. Sobczak *et al.*

Science **338**, 1458 (2012);
DOI: 10.1126/science.1229919

Science (print ISSN 0036-8075; online ISSN 1095-9203) is published weekly, except the last week in December, by the American Association for the Advancement of Science, 1200 New York Avenue NW, Washington, DC 20005.

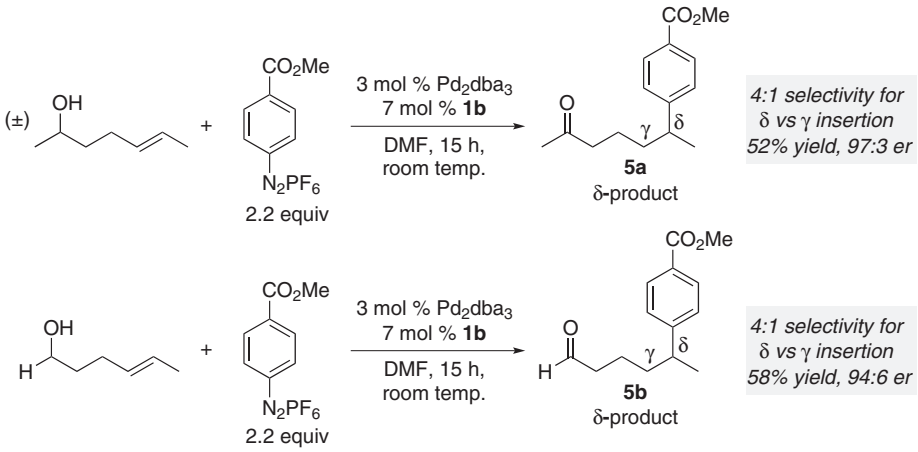

Fig. 5. Evaluation of bis-homoallylic alcohol substrates in the enantioselective Heck reaction.

alkene (Fig. 5). Under the same reaction conditions, the enantioselective Heck reaction successfully resulted in the formation of δ-substituted carbonyl products **5a** and **5b**. The selectivity of insertion is diminished somewhat with ~20% of the γ-substituted product observed. However, high enantioselectivity is still achieved, thus showcasing the robustness and potential power of the catalytic system.

The data presented suggest that the tactic of asymmetrically functionalizing alkenes and transferring unsaturation to a tethered functional group capable of being oxidized can be applied to the synthesis of remote chiral centers. Further studies will be required to establish what features of the catalyst contribute to high selectivity of the insertion events.

References and Notes

1. D. Mc Cartney, P. J. Guiry, *Chem. Soc. Rev.* **40**, 5122 (2011).
2. M. Shibasaki, E. M. Vogl, T. Ohshima, *Adv. Synth. Catal.* **346**, 1533 (2004).
3. A. B. Dounay, L. E. Overman, *Chem. Rev.* **103**, 2945 (2003).
4. M. S. Sigman, E. W. Werner, *Acc. Chem. Res.* **45**, 874 (2012).
5. K. Yonehara *et al.*, *J. Organomet. Chem.* **603**, 40 (2000).
6. K. S. Yoo *et al.*, *Org. Lett.* **9**, 3933 (2007).
7. K. S. Yoo *et al.*, *J. Org. Chem.* **75**, 95 (2010).
8. I. P. Beletskaya, A. V. Cheprakov, *Chem. Rev.* **100**, 3009 (2000).
9. J. B. Melpolder, R. F. Heck, *J. Org. Chem.* **41**, 265 (1976).
10. F. Berthiol, H. Doucet, M. Santelli, *Tetrahedron* **62**, 4372 (2006).
11. V. Calò, A. Nacci, A. Monopoli, V. Ferola, *J. Org. Chem.* **72**, 2596 (2007).
12. E. W. Werner, M. S. Sigman, *J. Am. Chem. Soc.* **132**, 13981 (2010).
13. E. W. Werner, M. S. Sigman, *J. Am. Chem. Soc.* **133**, 9692 (2011).
14. S. Bouquillon, B. Ganchegui, B. Estrine, F. Hénin, J. Muzart, *J. Organomet. Chem.* **634**, 153 (2001).
15. R. C. Larock, W.-Y. Leung, S. Stolz-Dunn, *Tetrahedron Lett.* **30**, 6629 (1989).
16. J. M. Richter *et al.*, *J. Am. Chem. Soc.* **130**, 17938 (2008).
17. N. Z. Burns, P. S. Baran, R. W. Hoffmann, *Angew. Chem. Int. Ed.* **48**, 2854 (2009).
18. K. B. Urkalan, M. S. Sigman, *Angew. Chem. Int. Ed.* **48**, 3146 (2009).
19. K. Kikukawa, K. Nagira, F. Wada, T. Matsuda, *Tetrahedron* **37**, 31 (1981).
20. J. G. Taylor, A. V. Moro, C. R. D. Correia, *Eur. J. Org. Chem.* **2011**, 1403 (2011).
21. A. Roglans, A. Pla-Quintana, M. Moreno-Mañas, *Chem. Rev.* **106**, 4622 (2006).
22. K. H. Jensen, T. P. Pathak, Y. Zhang, M. S. Sigman, *J. Am. Chem. Soc.* **131**, 17074 (2009).
23. B. W. Michel, A. M. Camelio, C. N. Cornell, M. S. Sigman, *J. Am. Chem. Soc.* **131**, 6076 (2009).
24. R. I. McDonald, P. B. White, A. B. Weinstein, C. P. Tam, S. S. Stahl, *Org. Lett.* **13**, 2830 (2011).
25. K. Kikushima, J. C. Holder, M. Gatti, B. M. Stoltz, *J. Am. Chem. Soc.* **133**, 6902 (2011).
26. K. C. Harper, M. S. Sigman, *Science* **333**, 1875 (2011).
27. K. C. Harper, E. N. Bess, M. S. Sigman, *Nat. Chem.* **4**, 366 (2012).
28. B. W. Michel, L. D. Steffens, M. S. Sigman, *J. Am. Chem. Soc.* **133**, 8317 (2011).
29. K. H. Jensen, J. D. Webb, M. S. Sigman, *J. Am. Chem. Soc.* **132**, 17471 (2010).
30. T. Hayashi, K. Yamasaki, *Chem. Rev.* **103**, 2829 (2003).
31. S. W. Smith, G. C. Fu, *J. Am. Chem. Soc.* **131**, 14231 (2009).
32. S. L. Zultanski, G. C. Fu, *J. Am. Chem. Soc.* **133**, 15362 (2011).
33. K. S. Ayyar, G. S. K. Rao, *Can. J. Chem.* **46**, 1467 (1968).
34. K. Tanaka *et al.*, *Chem. Pharm. Bull.* **47**, 1053 (1999).

Acknowledgments: Supported by NIH grant R01GM063540.

Supplementary Materials

www.sciencemag.org/cgi/content/full/338/6113/1455/DC1
Materials and Methods
Fig. S1
Tables S1 to S5
References (*35*–*51*)

23 August 2012; accepted 3 October 2012
10.1126/science.1229208

Rapid Folding of DNA into Nanoscale Shapes at Constant Temperature

Jean-Philippe J. Sobczak, Thomas G. Martin, Thomas Gerling, Hendrik Dietz*

We demonstrate that, at constant temperature, hundreds of DNA strands can cooperatively fold a long template DNA strand within minutes into complex nanoscale objects. Folding occurred out of equilibrium along nucleation-driven pathways at temperatures that could be influenced by the choice of sequences, strand lengths, and chain topology. Unfolding occurred in apparent equilibrium at higher temperatures than those for folding. Folding at optimized constant temperatures enabled the rapid production of three-dimensional DNA objects with yields that approached 100%. The results point to similarities with protein folding in spite of chemical and structural differences. The possibility for rapid and high-yield assembly will enable DNA nanotechnology for practical applications.

A candidate route toward the creation of synthetic nanodevices that achieve functionalities such as those of natural protein-based assemblies (*1*) relies on molecular self-assembly with DNA (*2*). Design strategies for encoding complex target shapes in DNA sequences have flourished (*3*–*15*), but the practical assembly of desired objects has often been quite difficult. Low yields and up to week-long reaction times have challenged, in particular, the usefulness of templated three-dimensional (3D) DNA objects in practical applications (*16*).

In our work, we used results from folding studies with templated DNA objects to find a solution to this problem. "Folding" herein refers to the association of multiple DNA strand species to form a user-defined object through hybridization into double-helical DNA domains, whereas "unfolding" denotes denaturation through strand dissociation. We used real-time fluorometric monitoring and cryogenic reaction quenching to study such folding and unfolding processes as a function of temperature and time (*17*). From the fluorometric data, we obtained a rate of folding during cooling a solution starting from denaturing temperatures, as well as a rate of unfolding during heating a solution containing folded objects. The rates measured changes in the solution

Physics Department, Walter Schottky Institute, Technische Universität München, Am Coulombwall 4a, 85748 Garching near Munich, Germany.

*To whom correspondence should be addressed. E-mail: dietz@tum.de

content of object-related DNA base pairs at a defined temperature (*18*). The cryogenic reaction quenching gave complementary insight into the shapes and electrophoretic mobilities of products contained in the reaction mixtures at specified time points and temperatures.

In a first set of experiments, one-pot reaction mixtures containing all required DNA strands were cooled stepwise, starting from denaturing temperatures, in analogy to previously reported protocols (*8*). We observed a rate of folding that featured a distinct peak at an object-specific temperature and that otherwise fluctuated around zero. Exemplary data obtained for three particular multilayer DNA objects—platelike (*19*), bricklike (*20*), and gearlike objects—are shown in Fig. 1, A to C. Results obtained for nontemplated DNA objects (*14*) are shown in the supplementary text. The data suggested that the plates began to fold only upon cooling to a temperature of 60°C and that their folding was completed at 55°C, whereas the bricks and gears folded within the interval from 55° to 50°C. Cryogenic reaction quenching during stepwise cooling followed by analysis by gel electrophoresis and transmission electron microscopy (TEM) imaging confirmed this interpretation (Fig. 1, D to F): At the high-temperature boundary of the peak in the rate-of-folding data, compacted "molten globule"–like (*21*) precursors with greater electrophoretic mobility than that of the unfolded species formed in all reactions (Fig. 1, D to F). Upon further cooling, folded objects appeared and coexisted with the precursors. The conversion to the folded state (as judged by electrophoretic mobility and TEM imaging) was completed at the low-temperature boundary of the peak in the rate-of-folding data.

In a second set of experiments, reaction mixtures containing previously folded DNA objects were heated stepwise. The rate of unfolding featured distinct peaks that were more narrow and shifted toward higher temperatures as compared with the peaks in the rate-of-folding data (Fig. 1, A to C). These data suggested that the objects remained folded up to higher temperatures compared with the temperatures at which they previously formed; this result was confirmed by cryogenic reaction quenching (Fig. 1, D to F). Because cooling and heating gave different results, the data pointed to nonequilibrium processes. Experiments in which folded objects were incubated for either 2 hours or 2 days at set temperatures within the peak in the rate-of-unfolding data gave unchanged results regarding the temperatures at which the objects unfolded (fig. S4B). By contrast, experiments in which unfolded objects were incubated for 2 days at set temperatures within the peak range in the rate-of-folding data led to folding at higher temperatures as opposed to 2-hour-long incubation (fig. S4A). Thus, folding rather than unfolding was not in equilibrium at the time scales that we tested.

The data also revealed strong cooperativity in folding and unfolding. For independent hybridization of full-length DNA strands to the template strand, base pairs are expected to form over a broad temperature range ($\Delta T > 30$°C) at temperatures well above 60°C. By contrast, for independent hybridization of all double-stranded DNA (dsDNA) domains designed in each object, base pairs are expected to also form over a broad temperature range ($\Delta T > 30$°C), but mostly at temperatures well below 45°C. Both cases were not observed; instead, all objects that we tested folded at intermediate temperatures between 45° and 60°C, and base pairs formed only within narrow temperature intervals ($\Delta T \sim 4$°C) (Fig. 1). Analogous reasoning applied to the observed cooperativity during unfolding.

In a third set of experiments, we studied the folding and unfolding of a hinged-bar–shaped object consisting of two independent domains organized on interleaved template strand segments. We observed domain-wide cooperative folding and unfolding, similar to in proteins (*22*, *23*): The two domains folded independently in two distinct folding transitions (Fig. 2A). TEM imaging of reaction products shock-frozen at the temperature between the two peaks in the rate-of-folding data revealed objects in which the longer "arm" domain was folded and an unstructured loop was hanging off, whereas reaction mixtures extracted at the lower-temperature boundary of both peaks contained fully folded hinged-bar objects (Fig. 2B). The unfolding of the hinged-bar

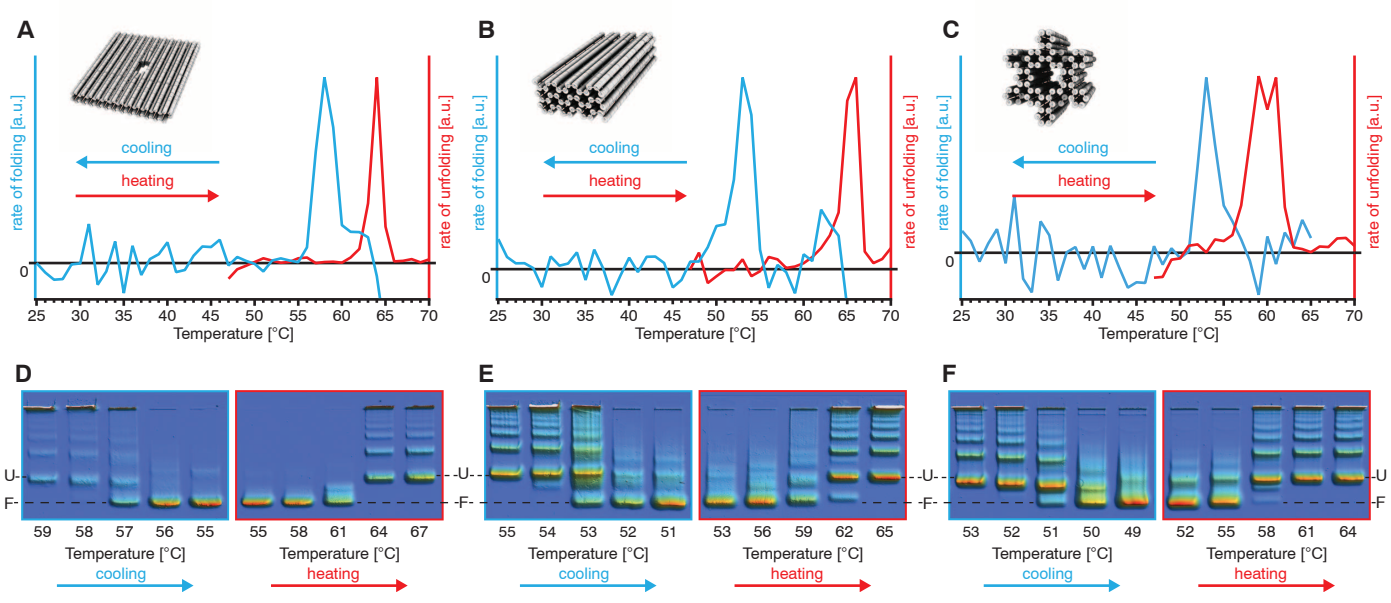

Fig. 1. Folding and unfolding of templated multilayer DNA objects as a function of temperature. (**A**) Fluorometrically obtained rates of folding (blue line) and unfolding (red line) for a templated multilayer platelike DNA object (inset). For folding, after a fluorescence equilibration period (*18*), one-pot reaction mixtures were denatured for 5 min at 65°C and then cooled stepwise to room temperature. The rate of cooling was 1 K per 15 min from 64° to 60°C and 1 K per 3 hours from 60° to 25°C. For unfolding, unpurified one-pot reaction mixtures containing previously folded objects were heated stepwise with a rate of 1 K per 3 hours. a.u., arbitrary units. (**B** and **C**) Same as in (A), but for templated bricklike and gearlike objects, respectively. (**D** to **F**) Agarose gel-electrophoretic mobility analysis of reaction products in temperature-resolved cryogenic shock-freezing experiments. (Left) One-pot reaction mixtures were subjected to stepwise cooling as in (A) to (C), but samples were extracted and shock-frozen in liquid nitrogen after the incubation step at the indicated temperatures was completed. (Right) Reaction mixtures containing folded objects were incubated for 2 hours at the temperatures indicated, then extracted and shock-frozen. U and F denote bands corresponding to unfolded and folded species, respectively. Bands in between the U and F markers correspond to compacted precursors (folding) or partially unfolded objects (unfolding). Gel photographs were depicted in 3D landscape mode to support the comparison of band intensities. Source data in grayscale are given in fig. S5. See figs. S9 to S12 for additional TEM data and figs. S19 to S21 for design details. Sequences are given in tables S1 to S3.

object upon heating also occurred in two steps: First the short arm of the object unfolded, followed by unfolding of the long arm (Fig. 2C).

In a fourth set of experiments, we explored the influence of design details on the folding and unfolding transitions of the same overall shape (a bricklike object). Assuming that nuclei for folding consist of the dsDNA domains with the highest independent thermal stability as defined by design, template sequence permutations will influence the pathways available for nonequilibrium folding and, thus, affect the temperatures at which folding occurs. By contrast, for near-equilibrium unfolding, the temperatures at which sequence variants of an object unfold should be similar, because the total number and composition of base pairs will be identical. We observed this behavior for sequence variants of the bricklike object (Fig. 2, D and E). Single-nucleotide mismatches in all dsDNA domains defined in the bricklike object led to failure to fold, as reflected in a missing peak in the fluorometric rate-of-folding trace (Fig. 2F). Increasing the average length of staple strands from 42 to 100 bases led to a broadening and shifting toward higher temperatures of the peak in the rate of folding, but had little influence on the rate of unfolding (Fig. 2G). Additional energetic penalties—for instance, bending (*9*)—are expected to lead to destabilization and, thus, to a shift of folding and unfolding transitions to lower temperatures. We observed this result for a moderately bent version of the bricklike object (Fig. 2, H and J). A strongly bent version did not fold anymore, as seen in TEM data and in the loss of a distinct peak in the rate-of-folding trace (Fig. 2, I and K). Finally, varying the staple-strand routing while using identical template-strand routing and sequence permutation influenced both folding and unfolding transitions of the bricklike object in various ways (fig. S7). Thus, design choices shifted folding and unfolding temperatures both together and independently for the same shape, which may allow for rationally tuning DNA objects to assemble and disassemble at target temperatures.

Given the high degree of cooperativity and the sharply defined transition temperatures for folding templated DNA objects, we hypothesized that such objects might be capable of folding at constant temperature, thus dispensing with annealing (*3*–*15*, *24*). A fifth set of experiments revealed that this was true (Fig. 3 and fig. S8). At the low-temperature boundary T_{fold} of the peak in the object-specific, rate-of-folding data, the process of folding occurred on a time scale of minutes. Deviating from this optimal T_{fold} slowed down or inhibited folding entirely (Fig. 3A and fig. S8, A and G). Folded DNA plates, bricks, and gears appeared in the reactions after 15, 30, and 40 min, respectively, of incubation at constant T_{fold}, as seen in time-resolved cryogenic reaction-quench experiments (Fig. 3C and fig. S8, C and G). Note that prior thermal denaturation by a heat shock (e.g., 15 min at 65°C), presumably to resolve secondary structures in the template strand, was obligatory to achieve folding. As in the stepwise cooling experiments in Fig. 1, the objects folded across compacted precursors at constant T_{fold}. Unfolding at the temperature of the peak in the rate-of-unfolding data occurred rapidly within seconds (Fig. 3D and fig. S8, D and H). Time-resolved fluorometric data indicated reaction completion at comparable time scales, as seen for folding and unfolding in the cryogenic experiments (Fig. 3, E and F). Thus, the time scales for folding may also be determined using the more convenient, parallelizable fluorometric assay. A templated single-layer DNA object folded at 53°C within 5 min (Fig. 3, G to J). Finally, constant-temperature folding at T_{fold} strongly enhanced the yield of correctly folded particles (Fig. 3, K and L) by avoiding side-product formation and reducing material loss through thermal degradation. When reaction quality was measured electrophoretically by the ratio of leading band intensity (reflecting desired monomeric folded objects) versus aggregate band intensity, a 330-fold improvement over previous protocols (*8*) could be achieved for the gearlike object (Fig. 3K) (215-fold and sevenfold improvements for the DNA brick and plate objects, respectively). The absolute yield approached 100% when we compared folded particles with total particles that were seen in TEM images of excess-staple–freed, but not otherwise purified, reaction products (Fig. 3L and figs. S15 to S18). Note that these results were achieved in reactions that lasted 1% of the duration of previous protocols for making such objects (*8*).

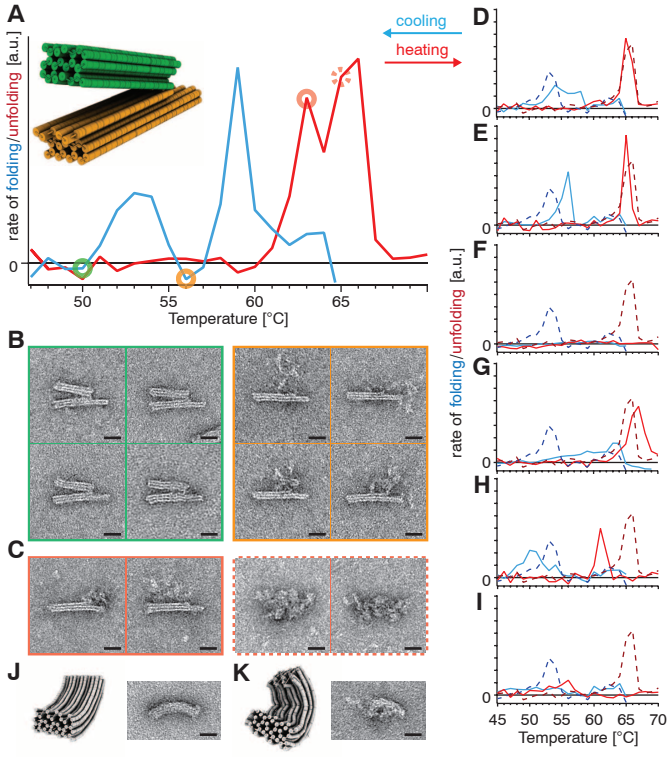

Fig. 2. Domain-wide folding cooperativity and the influence of design details on folding and unfolding temperatures. (**A**) Fluorometric rate of folding (blue line) upon cooling and rate of unfolding (red line) upon heating obtained for a templated DNA object shaped like a hinged bar. (**B**) Typical TEM micrographs of particles contained in hinged-bar reaction mixtures upon cooling, as in (A), that were shock-frozen at 56°C (right) and at 50°C (left). Scale bars, 20 nm. (**C**) Same as in (B), but from reheating folded objects and shock-freezing at 63°C (left) and at 65°C (right). Scale bars, 20 nm. (**D** to **G**) Fluorometric rate of folding (solid blue lines) upon stepwise cooling and the rate of unfolding (solid red lines) upon stepwise reheating of the formerly cooled reaction mixtures, as obtained for design variants of the bricklike object from Fig. 1. Results for the original version are given as dashed lines. (D and E) Sequence permutations. (F) Single-nucleotide mismatches in all double-helical DNA domains. (G) Average staple-strand length: 100 bases instead of 42. (**H** and **I**) Same as in (D) to (G), but for bent bricklike objects. (**J**) Typical TEM micrograph of a folded bricklike object from (H) with a moderate bend. Scale bar, 20 nm. (**K**) Same as in (J), but for a bricklike object designed with strong bend, which failed to fold. Scale bar, 20 nm. See figs. S13 and S14 for additional TEM data and figs. S22 to S27 for design details. Sequences are given in tables S4 to S16.

The possibility for rapid, high-yield production of complex DNA objects will support achieving usefulness of DNA nanotechnology in practical applications. Fine-tuning of DNA devices through serial cycles of functional selection (*25*) becomes practically feasible, and prospects for the hierarchical assembly (*8*, *26*–*28*) of larger objects are opened, where a high yield of well-folded building blocks is one important prerequisite. Furthermore, the finding that complex DNA objects are capable of folding at tunable constant temperatures within the lifetime of a cell suggests that assembly of such objects in cell culture or even within a cell may be possible.

References and Notes

1. B. Alberts *et al.*, *Molecular Biology of the Cell* (Garland Science, New York, ed. 5, 2002).
2. N. C. Seeman, *Annu. Rev. Biochem.* **79**, 65 (2010).
3. W. M. Shih, J. D. Quispe, G. F. Joyce, *Nature* **427**, 618 (2004).
4. P. W. K. Rothemund, *Nature* **440**, 297 (2006).
5. S. M. Douglas, J. J. Chou, W. M. Shih, *Proc. Natl. Acad. Sci. U.S.A.* **104**, 6644 (2007).
6. Y. Ke *et al.*, *Nano Lett.* **9**, 2445 (2009).
7. E. S. Andersen *et al.*, *Nature* **459**, 73 (2009).
8. S. M. Douglas *et al.*, *Nature* **459**, 414 (2009).
9. H. Dietz, S. M. Douglas, W. M. Shih, *Science* **325**, 725 (2009).
10. Y. Ke *et al.*, *J. Am. Chem. Soc.* **131**, 15903 (2009).

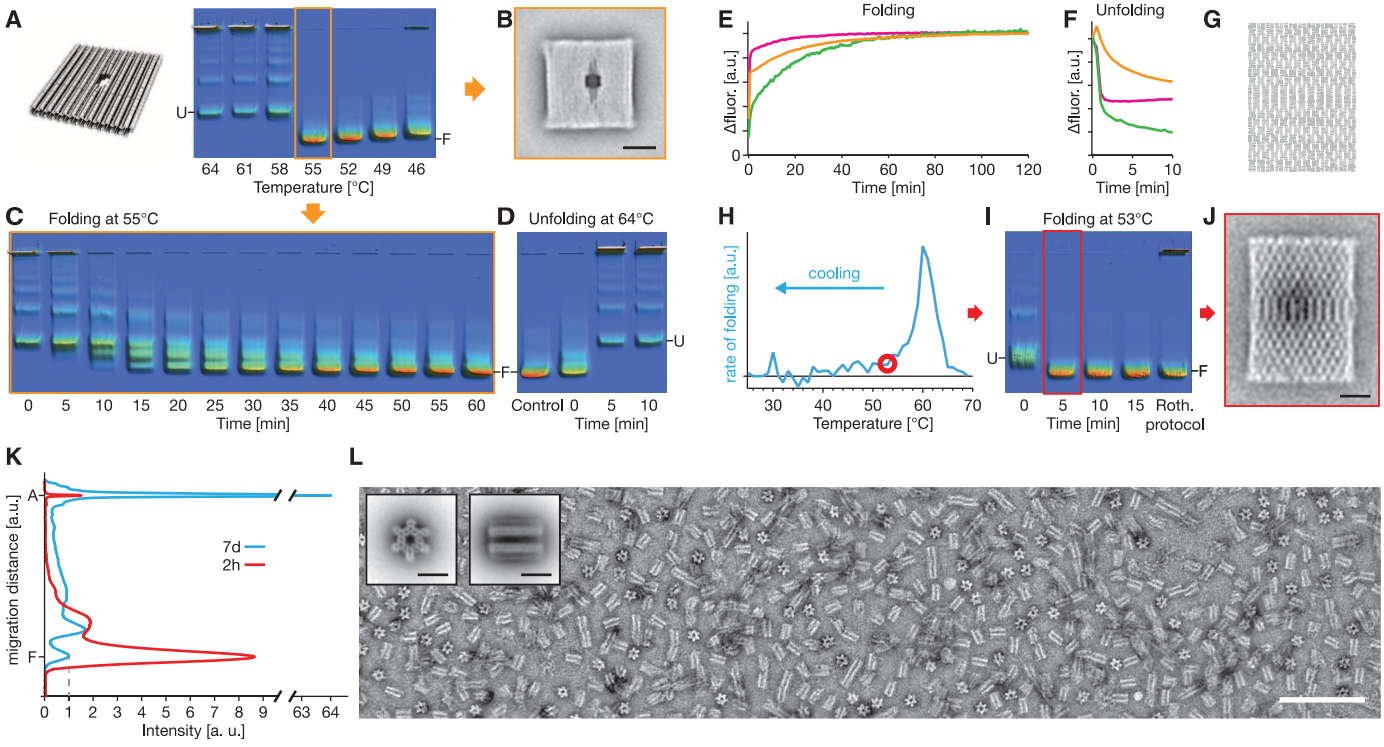

Fig. 3. Time-resolved folding and unfolding of templated DNA objects at constant temperature. (**A**) Agarose gel mobility analysis of products in reaction mixtures for the platelike object that were incubated for 2 hours at the temperatures indicated. (**B**) Averaged single-particle TEM micrograph obtained from excess-staple–free but not otherwise purified products in the boxed reaction in (A). Scale bar, 20 nm. See fig. S9 for additional TEM data. (**C**) Time-resolved folding of the platelike object at constant 55°C, as obtained through shock-freezing followed by agarose gel electrophoresis. (**D**) Time-resolved unfolding at constant 64°C. (**E**) Temporal evolution of the normalized SG fluorescence intensity in full assembly reaction mixtures minus intensity recorded in staple-only assembly reaction mixtures for DNA plates (orange) at 55°C, bricks (green) at 50°C, and gears (magenta) at 49°C. (**F**) Same as in (E), but for unfolding at the temperatures indicated in (D), fig. S8D, and fig. S8H, respectively. (**G**) Model of a templated 2D DNA rectangle [adapted from (*4*)]. (**H**) Rate of folding obtained upon stepwise cooling of the rectangle. (**I**) Time-resolved folding as in (C) and fig. S8, C and G, at 53°C of the rectangle object after prior denaturation at 95°C for 1 min. Roth. protocol denotes the lane on which products obtained using a previous protocol (*4*) were electrophoresed. Note the absence of aggregates in the boxed lane. (**J**) Averaged TEM micrograph of particles observed in the boxed reaction in (I). Scale bar, 20 nm. Note the correspondence to (G). (**K**) Comparison of gel-electrophoretic lane intensity profiles obtained for products from 2-hour constant-temperature folding (red line) versus annealing as in (*8*) (blue line) for the gearlike object. "A" denotes aggregates stuck in the gel pocket; "F" indicates folded objects. (**L**) Field-of-view negative-stain TEM micrograph of unpurified DNA gear reaction products (stripped from excess staple strands by filtration, but not otherwise purified). Black scale bars, 20 nm; white scale bar, 200 nm. See fig. S8 for an analysis, as in (A) to (D), for the bricklike and gearlike objects. Also see figs. S14 to S18 for field-of-view TEM data for plate-, brick-, and gearlike objects.

11. T. Liedl, B. Högberg, J. Tytell, D. E. Ingber, W. M. Shih, *Nat. Nanotechnol.* **5**, 520 (2010).
12. D. Han *et al.*, *Science* **332**, 342 (2011).
13. Y. Ke, N. V. Voigt, K. V. Gothelf, W. M. Shih, *J. Am. Chem. Soc.* **134**, 1770 (2012).
14. B. Wei, M. Dai, P. Yin, *Nature* **485**, 623 (2012).
15. S. M. Douglas, I. Bachelet, G. M. Church, *Science* **335**, 831 (2012).
16. A. V. Pinheiro, D. Han, W. M. Shih, H. Yan, *Nat. Nanotechnol.* **6**, 763 (2011).
17. In the fluorometric experiments, trace amounts of the organic dye SYBR green (SG) were added to one-pot self-assembly reaction mixtures (*18*). The use of low concentrations of SG corresponding to one SG molecule per ~900 possible DNA base pairs in solution ensured negligible perturbation of the DNA hybridization processes. The fluorescence brightness of SG is enhanced upon intercalation into dsDNA domains (*29*); recording the SG fluorescence intensity can thus provide a measure for the evolution of the overall content of DNA base pairs in solution. A specific signal for the formation of object-related DNA base pairs upon incubation for time *t* at temperature *T* is obtained by comparison with reference reactions (*18*). For templated DNA objects—i.e., objects that form by staple DNA strand–assisted folding of a much longer scaffold DNA template molecule (*4*)—reference reactions were prepared that included the respective set of staple DNA oligonucleotides but lacked the scaffold DNA strand. Cryogenic shock-freezing of a reaction mixture in liquid nitrogen quenched folding and unfolding processes and preserved the state of the reaction at the time and temperature of freezing (*18*). After quick thawing, the solution content was analyzed using agarose gel electrophoresis and/or direct imaging with negative-stain TEM. Gel electrophoresis and TEM imaging were performed as previously described (*30*). Excess staple strands were removed by molecular weight cut-off filtration with 100-kD spin filters. Objects were designed using caDNAno (*31*); models were computed using CanDo (*30*, *32*).
18. Materials and methods are available as supplementary materials on *Science* Online.
19. R. Wei, T. G. Martin, U. Rant, H. Dietz, *Angew. Chem. Int. Ed. Engl.* **51**, 4864 (2012).
20. T. G. Martin, H. Dietz, *Nat. Commun.* **3**, 1103 (2012).
21. M. Ohgushi, A. Wada, *FEBS Lett.* **164**, 21 (1983).
22. P. L. Privalov, *Annu. Rev. Biophys. Biophys. Chem.* **18**, 47 (1989).
23. L. L. Porter, G. D. Rose, *Proc. Natl. Acad. Sci. U.S.A.* **109**, 9420 (2012).
24. R. Jungmann, T. Liedl, T. L. Sobey, W. M. Shih, F. C. Simmel, *J. Am. Chem. Soc.* **130**, 10062 (2008).
25. G. F. Joyce, *Annu. Rev. Biochem.* **73**, 791 (2004).
26. S. Woo, P. W. K. Rothemund, *Nat. Chem.* **3**, 620 (2011).
27. J. Zheng *et al.*, *Nature* **461**, 74 (2009).
28. W. Liu, H. Zhong, R. Wang, N. C. Seeman, *Angew. Chem. Int. Ed. Engl.* **50**, 264 (2011).
29. H. Zipper, H. Brunner, J. Bernhagen, F. Vitzthum, *Nucleic Acids Res.* **32**, e103 (2004).
30. C. E. Castro *et al.*, *Nat. Methods* **8**, 221 (2011).
31. S. M. Douglas *et al.*, *Nucleic Acids Res.* **37**, 5001 (2009).
32. D. N. Kim, F. Kilchherr, H. Dietz, M. Bathe, *Nucleic Acids Res.* **40**, 2862 (2012).

Acknowledgments: This work was supported by the Deutsche Forschungsgemeinschaft through the Excellence Cluster CIPSM and the SFB863, the Technische Universität München Institute for Advanced Study, and a European Research Council Starting Grant to H.D. (GA no. 256270). We thank E. Lin Shiao for preliminary experiments, M. Schickinger for the design of the gearlike object, C. Castro for the design of the hinged-bar object, F. Praetorius for preparing scaffold DNA, and B. Wei and P. Yin for supplying DNA strands for tile-based DNA objects. Additional data described in this work can be found in the online supplementary materials.

Supplementary Materials

www.sciencemag.org/cgi/content/full/338/6113/1458/DC1
Materials and Methods
Supplementary Text
Figs. S1 to S34
Tables S1 to S17
References

10 September 2012; accepted 31 October 2012
10.1126/science.1229919